$Au_{133}(SPh\text{-}tBu)_{52}$ Nanomolecules: X-ray Crystallography, Optical, Electrochemical and Theoretical Analysis

Amala Dass,[1,*] Shevanuja Theivendran,[1,†] Praneeth Reddy Nimmala,[1,†] Chanaka Kumara,[1] Vijay Reddy Jupally,[1,§] Alessandro Fortunelli,[2] Luca Sementa,[2,†] Giovanni Barcaro,[2,†] Xiaobing Zuo[3], Bruce C. Noll,[4]

[1] Department of Chemistry and Biochemistry, University of Mississippi, Oxford, MS 38677, USA
[2] CNR-ICCOM & IPCF, Consiglio Nazionale delle Ricerche, Pisa, I-56124, Italy
[3] X-ray Science Division, Advanced Photon Source, Argonne National Laboratory, Argonne, Illinois 60439, USA
[4] Bruker AXS Inc., 5465 Cheryl Parkway, Madison WI 53711, USA

[§] Current address: Intel Corporation, 2501 NW 229th Avenue, Hillsboro, OR 97124, USA

Supporting Information Placeholder

ABSTRACT: Crystal structure determination has revolutionized modern science in biology, chemistry and physics. However, the difficulty in obtaining periodic crystal lattices which are needed for X-ray crystal analysis has hindered the determination of atomic structure in nanomaterials, known as the 'nanostructure problem'. Here, by using rigid and bulky ligands, we have overcome this limitation, and successfully solved the X-ray crystallographic structure of the largest reported thiolated gold nanomolecule, $Au_{133}S_{52}$. The total composition, $Au_{133}(SPh\text{-}tBu)_{52}$, was verified using high resolution electrospray ionization mass spectrometry (ESI-MS). The experimental and simulated optical spectra show an emergent surface plasmon resonance that is more pronounced than in the slightly larger $Au_{144}(SCH_2CH_2Ph)_{60}$. Theoretical analysis indicates that the presence of rigid and bulky ligands is the key to the successful crystal formation.

Gold nanomolecules or nanocrystal molecules [1] are ultrasmall, typically <3-nm, thiolated gold nanoparticles with a precise number of metal Au atoms and protecting organic thiolate ligands. These compounds possess unique electrochemical [2] and optical properties [3] which make them promising in a variety of applications, ranging from catalysis to biomedicine.[4] However, a deeper understanding of structure-property relationships for these materials is hindered by the difficulties in determining their crystal structure due to the nanostructure problem,[5] especially for the larger compounds which are the most appealing for many applications. While some crystal structures have been reported,[6-8] these are mostly of smaller sizes, with the largest compound being $Au_{102}(SC_6H_4\text{-}COOH)_{44}$. The X-ray crystal structure of the larger, stable and robust $Au_{144}(SCH_2CH_2Ph)_{60}$ nanomolecule is still an *unresolved* mystery, although it has been sought after for more than a decade.

Herein we report: a) the crystal structure of an unprecedentedly large Au thiolate $Au_{133}S_{52}$ nanomolecule, using a rigid and bulky aromatic ligand, with a precise number of Au metal atoms and organic ligands and exhibiting a peculiar hybrid structure reported here for the first time; b) isolating this mo-

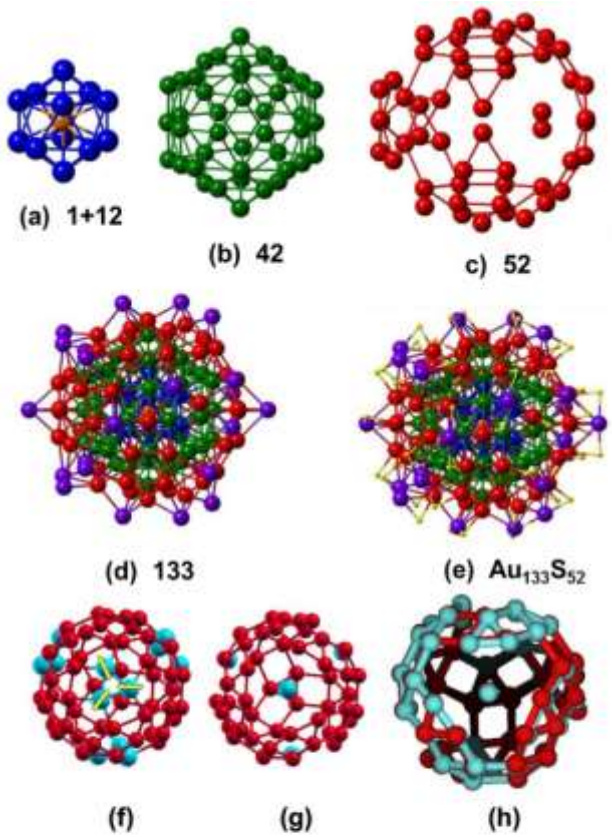

Figure 1. X-ray crystallographic structure of the $Au_{133}S_{52}$ core of $Au_{133}(SPh\text{-}tBu)_{52}$ nanomolecules. (a) Au_{12} icosahedral shell surrounding the central Au atom; (b) Au_{42} icosahedral shell; (c) 52-atom shell whose structure is derived from a 60-atom rhombiicosidodecahedron with 8 atoms missing; (d) Au_{133} core geometry showing the outmost 26 atoms that are part of the 26 [-SR-Au-SR-] units; (e) $Au_{133}S_{52}$ structure.; (f) merging of four Au_3 triangles (colored in light blue) in the 60-atom rhombicosahedral shell into single Au atom; (g) 52-atom shell resulting from step (f); (h) minor rearrangement of the 52-atom shell to produce the final structure, coinciding with that of (c), with initial positions in red and final positions in light blue.

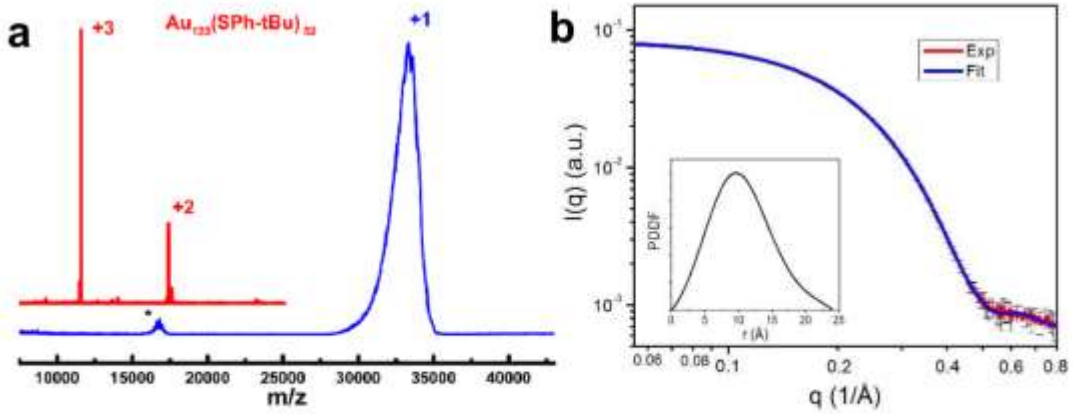

Figure 2. (a) Mass Spectrometry. MALDI (blue) and ESI (red) mass spectra of Au_{133}(SPh-*t*Bu)$_{52}$ nanomolecules. (b) X-ray scattering data (red curve with black error bars), GNOM fitting(*13*) (blue) and pair distance distribution function (PDDF, inset).

lecular substance in large quantity and verifying its composition using ESI and MALDI MS; c) characterizing its optical and electrochemical properties; and d) developing a theoretical analysis of the full Au_{133}(SPh-*t*Bu)$_{52}$ nanomolecule elucidating its electronic structure, geometrical and optical properties, thus achieving a consistent picture of its structure and properties through an excellent agreement of theoretical and experimental data and clarifying the reasons for its successful crystal formation.

The structure of Au_{133}(SPh-*t*Bu)$_{52}$ nanomolecule was solved in the C2/c space group to a R_1 value of 8.39% (table S1). Figure 1 shows the atomic structure of the metal-sulfur core, $Au_{133}S_{52}$. The structure consists of a central Au atom, surrounded by 12 Au atoms along the vertices of an icosahedron, Figure 1(a). This Au_{12} shell is covered by a second Au_{42} shell also in an icosahedral configuration, Figure 1(b), further enclosed by a Au_{52} shell, which is derived from the 60-atom rhombicosidodecahedron [9] lacking 8 atoms, Figure 1(c). The final layer is composed of $Au_{26}(SR)_{52}$, or 26 units of [-SR-Au-SR-] staples, Figure 1(d,e). The coordinates of the –Ph-*t*Bu ligands were not fully determined by X-ray data(see SI for details), due to the difficulty in accounting for organic ligands in large clusters as reported before e.g. for Pd systems[10], but the total composition including the ligands was confirmed using mass spectrometry and theoretical calculations, *vide infra*. The Au_{55} core (1+12+42 atoms) with a complete 60-atom rhombicosidodecahedral shell were first observed in Pd_{145} and Pd_{165} structures reported by Dahl's group,[9,10] and are the basis for the proposed Au_{144} structural model.[11]

However, the geometry of the present Au_{107} core structure is peculiarly transformed from a rhombicosidodecahedron into a hybrid structure which to the best of our knowledge is reported here for the first time. This is obtained by first merging 4 Au triangles from the Au_{60} shell (whose centers lie at the vertex of a tetrahedron) into single Au atoms – see Fig. 1f. This reduces the steric hindrance of the bulky SPh-*t*Bu ligands but lowers the point group symmetry from I_h to T. A minor rearrangement of the Au_{52} shell further lowers the symmetry to a chiral D_2 structure – see Fig. 1g-h. Especially *the central Au atom is unexpected* given the widely accepted Au_{144} theoretical model which contains a Au_{12} core with no central atom.[12]

The core of Au_{133} nanomolecule is organized in shells: the first shell is occupied by a central Au atom and the second shell corresponds to an icosahedron of 12 vertexes; the third shell contains 42 atoms which are positioned both on-top of the 12 corners and at the middle of the 30 edges of the inner 12-atom icosahedron; the structure obtained is the well-known Mackay icosahedron of 55 atoms. A further growth of 60 atoms will lead to the formation of the 115-atom dodecahedron with full Ih symmetry observed in the Pd_{145} structure[10]; this growth mode corresponds to the occupation of the anti-Mackay sites by the outer gold atoms, which would occupy all the 60 hollow sites of the inner 55-atom icosahedron. On the other hand, in the 133-Au atom structure only 52 atoms are found in the fourth shell, with a peculiar reconstruction which lowers the symmetry from Ih to a chiral D2, which, to the best of our knowledge, is reported here for the first time. This reconstruction can be seen in two steps: (i) a merging of 4 Au triangles from the Au_{60} shell (whose centers lie at the vertex of a tetrahedron) into single Au atoms – see Fig. 1f; this reduces the steric hindrance of the bulky SPh-tBu ligands but lowers the point group symmetry from Ih to T; (ii) a subsequent minor rearrangement of the Au_{52} shell further lowers the symmetry to the chiral D_2 structure – see Fig. 1g-h. A final fifth shell of 26 atoms - instead of 30, as in the case of Pd_{145} compound - completes the structure of the gold core with a complete loss of symmetry. The greater sparsity in the last two shells correspond to a slight contraction of the shell radii; by comparing the present structure with the powder XRD from ref. [12], we observe the following values: in the fourth shell of 52 atoms of the 133-Au atom structure, an average radius of 6.87 Å with respect to a radius of 7.10 Å for the 60-atom shell of the theoretically predicted Au_{144} model; in the fifth shell of 26 atoms of the 133-Au atom structure, an average radius of 8.47 Å with respect to a radius of 9.03 Å for the 30-atom shell of the 144-Au atom model.

Au_{133}(SPh-*t*Bu)$_{52}$ was synthesized, purified using size exclusion chromatography in large quantities and its composition and purity was verified using mass spectrometry[13]. In Figure 2a, the blue curve shows the MALDI-MS using DCTB matrix,[14] with one broad dominant feature centered ~33,000 m/z, and a minor feature centered ~16,000 m/z, corresponding to the singly and doubly charged molecular ions, respectively. ESI-MS, shown in the red spectrum in Figure 2a, contains two peaks at 11,596.7 and 17,395.8 m/z corresponding to the 3+ and 2+ ions

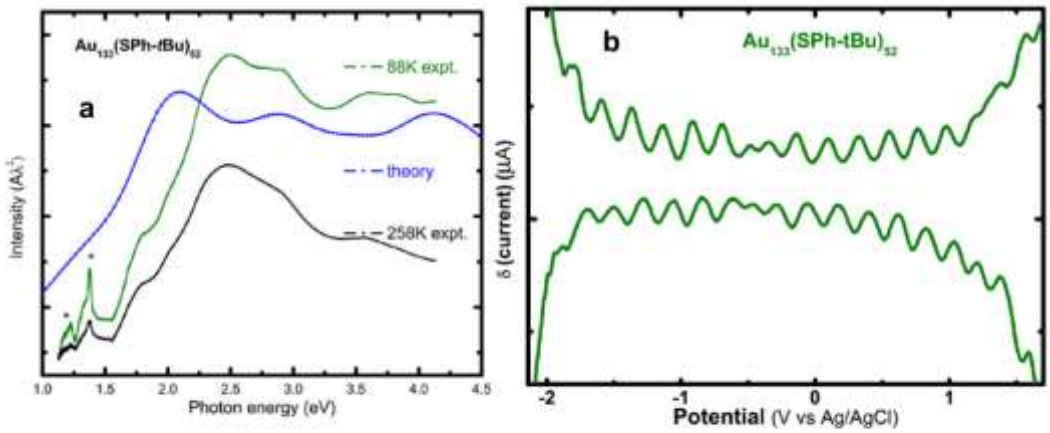

Figure 3. (a) UV-vis spectrum of $Au_{133}(SPh\text{-}tBu)_{52}$ nanomolecules in 3-MeTHF at 258K (black) and 88K (green). Theoretically predicted TDDFT spectrum is shown in blue (b) Electrochemical differential pulse voltammetry (DPV) of $Au_{133}(SCH_2Ph\text{-}tBu)_{52}$.

of $Au_{133}(SPh\text{-}tBu)_{52}$, respectively. The theoretical values for the 3+ and 2+ ions are 11,596.8 and 17,395.2 m/z, with a mass error of 8 and 34 ppm respectively. Intentional addition of cesium acetate[13] resulted in $[Au_{133}(SPh\text{-}tBu)_{52} \bullet 2Cs^+]^{3+}$ as a major adduct, indicating that the +1 is the preferred charge state in agreement with theoretical analysis, *vide infra*. MALDI-MS (Fig. 2a), including the expanded mass range (fig. S3), and at very high laser fluence (fig. S4, S5) show that the final product is highly pure, without any other core sizes. Unfragmented and high resolution ESI MS yields the $Au_{133}(SPh\text{-}tBu)_{52}$ composition, confirming the crystallographic results. Additional supporting evidence for the nanoparticle size, and purity were provided by small-angle x-ray scattering (SAXS) and transmission electron microscopy (TEM) (fig. S1). SAXS data fitting up to 0.8Å shows that the diameter is in agreement with MS and X-ray results (Fig. 2b) and the uniform size was demonstrated by the wide range of linear Guinier behavior ($\ln[I(q)]$ vs q^2 (fig. S6).

The optical spectra at two different temperatures, shown in Figure 3(a), displays distinct features[3] at 2.49 eV and between 3.59 and 3.81 eV, with a secondary peak at 2.91 eV. The peaks at 2.49 and 2.91 eV are reminiscent of the surface plasmon resonance, and are more pronounced than in $Au_{144}(SCH_2CH_2Ph)_{60}$[15]. Differential pulse voltammogram, Figure 3(b), shows 17 distinct redox waves more than the 15 waves[16] reported for $Au_{144}(SCH_2CH_2Ph)_{60}$, whose positions are different than those of Au_{130} or Au_{144}.[2]

Theoretical analysis fully supports the experimental assignment and provides a framework for the interpretation of experimental results. Starting from the experimental X-ray geometry of the $Au_{133}S_{52}$ core, –Ph-*t*Bu groups were added and this initial structure was subjected to local relaxation followed by two 1 psec runs of ab initio Molecular Dynamics (AIMD) based on a density-functional theory (DFT) approach(17): a first AIMD run at 900 K to allow the initial guess to exit possible meta-stable local minima, and a second AIMD run at 300 K to produce equilibrated coordinates[13]. The geometry of $Au_{133}(SPh\text{-}tBu)_{52}$ obtained by a final local relaxation is shown in Figure 4 and is reported in the Supplementary Information.[13]

The –SPh-*t*Bu ligands play a crucial role in determining the structure. Replacement of non-bulky ligands as in $Au_{144}(SCH_2CH_2Ph)_{60}$ with bulkier phenyl groups in fact creates a steric repulsion in proximity of the Au cluster which is alleviated by decreasing the thiolate surface density,[17] with the average surface area per sulfur atom increasing from 18.8 Å^2 to 19.2 Å^2 in passing from $Au_{144}S_{60}$ to $Au_{133}S_{52}$. We estimate the residual steric repulsion in $Au_{133}(SPh\text{-}tBu)_{52}$ to be ≈1.6 eV via an energy decomposition analysis [18] [13] thus being minor in such a large compound. At this decreased thiolate surface density, the rigid *p*-tBu groups play an important role as they provide an outer protective layer which has the double effect of: (i) reducing the cluster structural freedom, and (ii) preventing exogenous species (e.g. solvent molecules) to adsorb on the surface of the Au cluster. Both these features allow a cleaner and better-defined crystal formation, facilitating the X-ray crystal structure determination and enhancing thermodynamic and kinetic stability of $Au_{133}(SPh\text{-}tBu)_{52}$.

The UV-vis optical spectrum from time-dependent DFT simulations is reported in Figure 3(a), and compares reasonably well with experimental: the features at 2.09, 2.87 and 4.1 eV are in tune with the experimental peaks at 2.49, 2.91 and [3.59–3.81] eV, with the feature at 2.09 eV red-shifted due to the use of the LDA xc-functional [19]. A comparison with the spectrum of $Au_{144}(SCH_2CH_2Ph)_{60}$ [15] indicates a less fragmented and more pronounced optical absorption of $Au_{133}(SPh\text{-}tBu)_{52}$, probably associated with increased polarizability due to the decreased thiolate density [20] and electron delocalization provided by phenyl conjugating. This is confirmed by a comparison with the simulated spectrum of a putative $Au_{133}(SCH_3)_{52}$ analogue (fig. S8) clearly exhibiting a greater fragmentation due to quantum size effects,[21] pointing to a non-negligible influence of conjugation onto the optical response of these systems.

The ionization energy of $Au_{133}(SPh\text{-}tBu)_{52}$ is modest, amounting to 4.34 eV, supporting the experimental observation of +1 as the predominant charge state (see also fig. S2). The electronic density of states of $Au_{133}(SPh\text{-}tBu)_{52}$ (fig. S7) is in tune with a count of 81 free electrons, and exhibits a small HOMO-LUMO gap of 0.05 eV, which increases to 0.11 eV in the $Au_{133}(SPh\text{-}tBu)_{52}^+$ cation, in excellent agreement with the lack of a band gap in voltammetry – Figure 3(b). No superatom electronic shell closure and related stability is observed:(*12, 22,23)* the stability of $Au_{133}(SPh\text{-}tBu)_{52}$ is due to the geometric reasons, [18,22] with the geometric shell closings [23] of 1+12+42+52 atoms (Figure 1). Indeed, the energy gain due to electronic

shell-closure should amount to no more than 0.5-0.6 eV at this size,[24,25] thus being minor with respect to geometric effects. *(17, 21)*

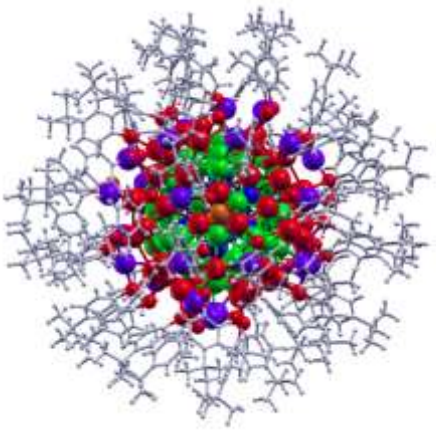

Figure 4. Theoretically predicted geometry of the $Au_{133}(SPh\text{-}tBu)_{52}$ nanomolecule. See text for more details. Color coding as in Figure 1, and C and H atoms are displayed in light gray.

The achievement of such an unprecedented size is theoretically rationalized as due to the presence of rigid and bulky –SPh-*t*Bu ligands which act as an outer protective layer, internally reducing the structural freedom of the cluster and externally preventing contamination by exogenous species. Employing bulky and rigid ligands may offer one solution to the nanostructure problem and facilitate the crystal structure determination of even larger nanomolecular materials.

ASSOCIATED CONTENT

Supporting Information

Detailed Synthetic conditions, additional mass spectra, theoretical analysis, crystal structure data and coordinates. This material is available free of charge via the Internet at http://pubs.acs.org.

AUTHOR INFORMATION

Corresponding Author

amal@olemiss.edu

Author Contributions

†These authors contributed equally.

Notes

The authors declare no competing financial interests.

ACKNOWLEDGMENT

This work was funded through NSF-CHE-1255519. We thank Ilia A. Guzei and Bruce Noll for assistance with crystal structure solution; Nanfeng Zheng and Jared Delcamp for discussions. Work performed at Argonne and use of the Advanced Photon Source, an Office of Science User Facility operated for the U.S. Department of Energy (DOE) Office of Science by Argonne National Laboratory, was supported by the U.S. DOE under Contract No. DE-AC02-06CH11357. Computational research was performed in part using EMSL, a DOE Office of Science User Facility sponsored by the Office of Biological and Environmental Research and located at Pacific Northwest National Laboratory.

REFERENCES

(1) Whetten, R. L.; Khoury, J. T.; Alvarez, M. M.; Murthy, S.; Vezmar, I.; Wang, Z. L.; Stephens, P. W.; Cleveland, C. L.; Luedtke, W. D.; Landman, U. *Adv. Mater.* **1996**, *8*, 428.
(2) Murray, R. W. *Chem. Rev.* **2008**, *108*, 2688.
(3) Alvarez, M. M.; Khoury, J. T.; Schaaff, T. G.; Shafigullin, M. N.; Vezmar, I.; Whetten, R. L. *J. Phys. Chem. B* **1997**, *101*, 3706.
(4) Daniel, M.-C.; Astruc, D. *Chem. Rev.* **2003**, *104*, 293.
(5) Billinge, S. J. L.; Levin, I. *Science* **2007**, *316*, 561.
(6) Jadzinsky, P. D.; Calero, G.; Ackerson, C. J.; Bushnell, D. A.; Kornberg, R. D. *Science* **2007**, *318*, 430.
(7) Heaven, M. W.; Dass, A.; White, P. S.; Holt, K. M.; Murray, R. W. *J. Am. Chem. Soc.* **2008**, *130*, 3754.
(8) Qian, H.; Zhu, M.; Wu, Z.; Jin, R. *Acc. Chem. Res.* **2012**, *45*, 1470.
(9) Mednikov, E. G.; Jewell, M. C.; Dahl, L. F. *J. Am. Chem. Soc.* **2007**, *129*, 11619.
(10) Tran, N. T.; Powell, D. R.; Dahl, L. F. *Angew. Chem. Int. Ed.* **2000**, *39*, 4121.
(11) Schaaff, T. G.; Shafigullin, M. N.; Khoury, J. T.; Vezmar, I.; Whetten, R. L. *J. Phys. Chem. B* **2001**, *105*, 8785.
(12) Lopez-Acevedo, O.; Akola, J.; Whetten, R. L.; Gronbeck, H.; Hakkinen, H. *J. Phys. Chem. C* **2009**, *113*, 5035.
(13) *See Supporting Information*.
(14) Dass, A.; Stevenson, A.; Dubay, G. R.; Tracy, J. B.; Murray, R. W. *J. Am. Chem. Soc.* **2008**, *130*, 5940.
(15) Weissker, H. C.; Escobar, H. B.; Thanthirige, V. D.; Kwak, K.; Lee, D.; Ramakrishna, G.; Whetten, R. L.; López-Lozano, X. *Nat Commun* **2014**, *5*.
(16) Quinn, B. M.; Liljeroth, P.; Ruiz, V.; Laaksonen, T.; Kontturi, K. *J. Am. Chem. Soc.* **2003**, *125*, 6644.
(17) Reimers, J. R.; Wang, Y.; Cankurtaran, B. O.; Ford, M. J. *J. Am. Chem. Soc.* **2010**, *132*, 8378.
(18) Crasto, D.; Barcaro, G.; Stener, M.; Sementa, L.; Fortunelli, A.; Dass, A. *J. Am. Chem. Soc.* **2014**, *136*, 14933.
(19) Perdew, J. P.; Burke, K.; Ernzerhof, M. *Phys. Rev. Lett.* **1996**, *77*, 3865.
(20) Sementa, L.; Marini, A.; Barcaro, G.; Negreiros, F. R.; Fortunelli, A. *ACS Photonics* **2014**, *1*, 315.
(21) Lermé, J.; Baida, H.; Bonnet, C.; Broyer, M.; Cottancin, E.; Crut, A.; Maioli, P.; Del Fatti, N.; Vallée, F.; Pellarin, M. *J. Phys. Chem. Lett.* **2010**, *1*, 2922.
(22) Dass, A. *Nanoscale* **2012**, *4*, 2260.
(23) Martin, T. P. *Physics Reports* **1996**, *273*, 199.
(24) Barcaro, G.; Fortunelli, A.; Rossi, G.; Nita, F.; Ferrando, R. *J. Phys. Chem. B.* **2006**, *110*, 23197.
(25) Ferrando, R.; Fortunelli, A.; Rossi, G. *Phys. Rev. B.* **2005**, *72*, 085449.

Insert Table of Contents artwork here

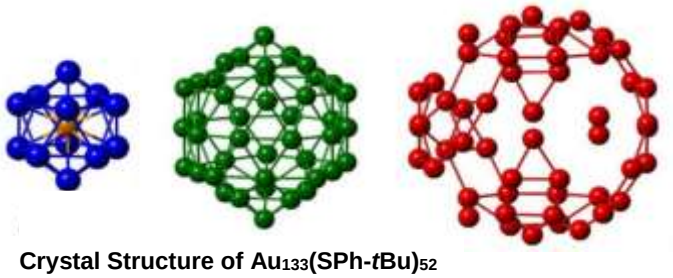

Crystal Structure of $Au_{133}(SPh\text{-}tBu)_{52}$